Standing wave approach in the theory of X-ray magnetic reflectivity

M. A. Andreeva,[a] R. A. Baulin[a]* and Yu. L. Repchenko[b]

[a]Faculty of Physics, M. V. Lomonosov Moscow State University, Moscow 119991, Russian Federation, and [b]National Research Centre 'Kurchatov Institute', Pl. Kurchatova 1, Moscow 123182, Russian Federation. *Correspondence e-mail: baulin.roman@physics.msu.ru

An extension of the exact X-ray resonant magnetic reflectivity theory has been developed, taking into account the small value of the magnetic terms in the X-ray susceptibility tensor. It is shown that squared standing waves (fourth power of the total electric field) determine the output of the magnetic addition to the total reflectivity from a magnetic multilayer. The obtained generalized kinematical approach essentially speeds up the calculation of the asymmetry ratio in the magnetic reflectivity. The developed approach easily explains the peculiarities of the angular dependence of the reflectivity with the rotated polarization (such as the peak at the critical angle of the total external reflection). The revealed dependence of the magnetic part of the total reflectivity on the squared standing waves means that the selection of the reflectivity with the rotated polarization ensures higher sensitivity to the depth profiles of magnetization than the secondary radiation at the specular reflection condition.

1. Introduction

Polarization properties of radiation absorbed or scattered by magnetized samples play more and more important roles in magnetic property investigations with synchrotron radiation. The modern synchrotron beamlines produce or create X-rays of any desired polarization state, and polarization-dependent absorption or scattering near the X-ray absorption edges (XMCD, XMLD, XMND, MχD, DAFS, XRMR) has become the basis of the extremely effective methods for magnetic or structure investigations (Brouder, 1990; Schütz *et al.*, 1994; Stöhr, 1995; Natoli *et al.*, 1998; Goulon *et al.*, 2003; van der Laan, 2013; Sessoli *et al.*, 2014). Polarization analysis in nonresonant magnetic X-ray scattering has proven to be a very effective tool for separating the charge and magnetic scattering [revealing, for example, the difference in charge and magnetic periodicity (Moncton *et al.*, 1986)], and determines the spin and orbital magnetic moments (Blume & Gibbs, 1988; Gibbs *et al.*, 1988; Bohr *et al.*, 1989; McWhan *et al.*, 1990; Bohr, 1990; Brückel *et al.*, 1996; Langridge *et al.*, 1997; Fernandez *et al.*, 1998; Neubeck *et al.*, 1999). Magneto-optical measurements (Faraday and Voigt effects) also utilized the polarization analysis of the transmitted radiation (Siddons *et al.*, 1990; Collins, 1999; Mertins *et al.*, 2000, 2001; Kortright & Kim, 2000). In resonant X-ray diffraction the selection of the $\sigma \rightarrow \pi'$ channel provides the possibility of enhancing fine effects like quadrupole transition contributions, orbital ordering, the Dzyaloshinskii–Moriya interaction and interference of the quadrupole resonant and nonresonant scattering amplitudes in structurally forbidden reflections (Caciuffo *et al.*, 2002; Takahashi *et al.*, 2003; Beutier *et al.*, 2017).
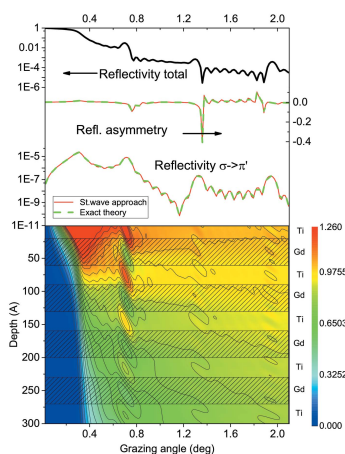
X-ray resonant magnetic reflectivity (XRMR) provides unique element, electronic shell and spatially selective information about the magnetic ordering in multilayer films (see, for example, Kao *et al.*, 1994; Tonnerre *et al.*, 1995; Gibert *et al.*, 2016; Brück *et al.*, 2008; Geissler *et al.*, 2001; Ishimatsu *et al.*, 1999; Sève *et al.*, 1999; Jaouen *et al.*, 2004; Hosoito *et al.*, 2009; Kim & Kortright, 2001; Valvidares *et al.*, 2008; Elzo *et al.*, 2015; Ott *et al.*, 2006; Bergmann *et al.*, 2006; Freeland *et al.*, 2010). In these experiments two circular or two linear polarizations of synchrotron radiation are used and the asymmetry ratio relative to the polarization state of the incident radiation is measured. The change of polarization of the reflected radiation (X-ray Kerr rotation) has been directly measured with soft X-rays in but a few works (Kortright & Rice, 1996; Oppeneer, 2001; Mertins *et al.*, 2004). Ellipsometry measurements have mainly been conducted in the visible range (Azzam & Bashara, 1977) but the usefulness of the ellipsometric investigations in the X-ray region has not been focused on until now. From the general point of view the polarization analysis of the reflected radiation should be a source of valuable information supplemented to the asymmetry ratio data. Moreover, as pointed out by Yamamoto *et al.* (2015) and Yamamoto & Matsuda (2017), following the development of femtosecond light sources such as synchrotron radiation sources using a laser slicing technique and free-electron lasers, the X-ray Kerr rotation is becoming increasingly important, particularly for temporal domain measurements on the subpicosecond timescale.

The polarization dependence of the reflectivity is obtained by exact calculations of the reflectivity matrix amplitude. Magnetic scattering, being significant near the absorption edges of magnetic atoms, radically complicates the theory of reflectivity, because the X-ray susceptibility of a medium becomes a tensor in the presence of magnetic scattering. The reflectivity theory from anisotropic (magnetic) multilayers has been developed (Ishimatsu *et al.*, 1999; Zak *et al.*, 1991; Bourzami *et al.*, 1999; Stepanov & Sinha, 2000; Elzo *et al.*, 2012) based on the eigen-wave formalism or by using the method of the 4×4 propagation matrices (see, for example, Azzam & Bashara, 1977; Borzdov *et al.*, 1976; Barkovskii *et al.*, 1983; Andreeva & Rosete, 1986; Andreeva & Smekhova, 2006; Andreeva *et al.*, 2006). The application of both algorithms for interpreting real experimental data is rather time-consuming; therefore, simplifying the calculations is a most urgent problem. In particular, analytical expressions were obtained for the 4×4-matrix integral propagation (Andreeva & Rosete, 1986; Pleshanov, 1994; Rühm *et al.*, 1999; Kravtsov *et al.*, 2009) using some simplifications which are not always valid (Odintsova & Andreeva, 2010). An interesting approach, namely a combination of dynamical (for the isotropic scattering part) and kinematical (for the magnetic scattering part) approximations, was used by Ott *et al.* (2006) to interpret the reflectivity curves near the Dy M_5 absorption edge for the dysprosium film revealing the helicoid magnetic ordering. A kinematic scalar approximation was used by Sève *et al.* (1999) and Jaouen *et al.* (2004) for interpreting the asymmetry ratio of the XRMR spectra to obtain the depth profiles of the spin polarization in the $5d$ electron shells of cerium and lanthanum in $[\mathrm{Ce/Fe}]_n$ and $[\mathrm{La/Fe}]_n$ multilayers. The polarization asymmetry ratio is generally very small and extremely sensitive to calculation errors. Correct interpretation of the experimental data is very important in such studies. It has been shown by Andreeva & Repchenko (2013) that the kinematic theory of reflectivity is applicable at angles far enough from the total reflection region but in some cases the complex polarization dependence of the propagating radiation leads to the wrong results even at rather large angles of incidence.

In this paper we show that the angular (and energy) dependence of the dichroic part of the magnetic contribution to the X-ray reflectivity is connected to the squared standing waves of the radiation inside the reflecting sample. It is mostly pronounced in the region of total external reflection and at other angles where the reflectivity is high enough. This finding explains the specific features of the angular dependence of the reflectivity with the rotated polarization and reveals the enhanced depth selectivity of this part of the reflectivity. In addition, the presented approach essentially simplifies the calculation of the reflectivity from magnetic multilayers. It implies the substitution of the complicated calculations with 4×4 propagation matrices (or eigen waves) by the simple Parratt algorithm for the isotropic part of the reflectivity and following integration of the magnetic part 'weighted' with the squared standing waves. We present some test calculations confirming the validity of the developed algorithm. The first experimental results of measuring the reflectivity with the rotated polarization are given.

2. X-ray reflectivity from an ultrathin layer

Reflectivity from an ultrathin layer r^d in the case of scalar susceptibility $\chi(z)$ can be easily obtained using the Parratt recurrent equations (Parratt, 1954),

$$R_{j-1,j} = \frac{r_{j-1,j} + R_{j,j+1}\,\tilde{R}\exp(2i\varphi_j)}{1 + r_{j-1,j}\,R_{j,j+1}\,\exp(2i\varphi_j)}, \tag{1}$$

where $2i\varphi_j = 2ik\eta_j d_j$, $\eta_j = (\sin^2\theta + \chi_j)^{1/2}$, χ_j and d_j are the scalar susceptibility and thickness of layer j, θ is the grazing angle, $r_{j-1,j} = (\eta_{j-1} - \eta_j)/(\eta_{j-1} + \eta_j)$ is the Fresnel amplitude reflectivity coefficient at the boundary between the $j-1$ and j layers, and $R_{j,j+1}$ is the amplitude reflectivity coefficient at the previous boundary taking into account the multiple reflections in the structure below.

If an ultrathin layer is detached in-vacuum, the Fresnel reflectivity coefficients from its boundaries are simply connected,

$$r_{01} = \frac{\sin\theta - \eta}{\sin\theta + \eta} = -r_{10} \tag{2}$$

[$\eta = (\sin^2\theta + \chi)^{1/2}$, χ is the susceptibility of the ultrathin layer], and supposing that the thickness of this layer d is very small we obtain the well known expression

$$r^d = \frac{r_{01} + r_{10}\exp(2i\varphi^d)}{1 + r_{01}\,r_{10}\exp(2i\varphi^d)} \cong \frac{r_{01} + r_{10}\,(1 + 2i\varphi^d)}{1 + r_{01}\,r_{10}\,(1 + 2i\varphi^d)}$$

$$\cong \frac{-r_{01}}{1 - r_{01}^2}2i\varphi^d = \frac{\eta^2 - \sin^2\theta}{4\sin\theta\,\eta}i2k\eta d = \frac{ikd\chi}{2\sin\theta}. \quad (3)$$

The most interesting result we obtain in the case when the layer is placed under some reflecting substrate. In this case the reflectivity from the whole system is calculated by the expression

$$R^{\mathrm{tot}} = \frac{r_{01} + \tilde{R}\exp(2i\varphi^d)}{1 + r_{01}\,\tilde{R}\exp(2i\varphi^d)}, \quad (4)$$

where

$$\tilde{R} = \frac{r_{10} + R^{\mathrm{substr}}\exp(iQH)}{1 + r_{10}\,R^{\mathrm{substr}}\exp(iQH)} \quad (5)$$

is the reflectivity from the bottom boundary of the film, $Q = (4\pi/\lambda)\sin\theta$, H is the distance from the substrate to the film, and R^{substr} is the reflectivity from the substrate (see Fig. 1).

Using the same expansion for $\exp(2i\varphi^d) \cong 1 + 2i\varphi^d$ as in (3), we obtain

$$R^{\mathrm{tot}} \cong \frac{r_{01} + \tilde{R}\,(1 + 2i\varphi^d)}{1 + r_{01}\,\tilde{R}\,(1 + 2i\varphi^d)}$$

$$= \frac{(r_{01} + \tilde{R}) + \tilde{R}\,2i\varphi^d}{(1 + r_{01}\,\tilde{R})\{1 + [(r_{01}\,\tilde{R}2i\varphi^d)/(1 + r_{01}\,\tilde{R})]\}}$$

$$\cong \frac{(r_{01} + \tilde{R}) + \tilde{R}2i\varphi^d}{(1 + r_{01}\,\tilde{R})}\left[1 - \frac{r_{01}\,\tilde{R}2i\varphi^d}{(1 + r_{01}\,\tilde{R})}\right]$$

$$\cong \frac{r_{01} + \tilde{R}}{1 + r_{01}\,\tilde{R}} + \frac{\tilde{R}\,(1 - r_{01}^2)}{(1 + r_{01}\,\tilde{R})^2}\,2i\varphi^d, \quad (6)$$

because $\tilde{R}(1 + r_{01}\tilde{R}) - r_{01}\tilde{R}(r_{01} + \tilde{R}) = \tilde{R}(1 - r_{01}^2)$.

After substituting (5) into (6), the first term in (6) is simplified to

$$\frac{r_{01} + [(r_{10} + R)/(1 + r_{10}R)]}{1 + r_{01}[(r_{10} + R)/(1 + r_{10}R)]} = \frac{r_{01}(1 + r_{10}R) + (r_{10} + R)}{(1 + r_{10}R) + r_{01}(r_{10} + R)} = R \quad (7)$$

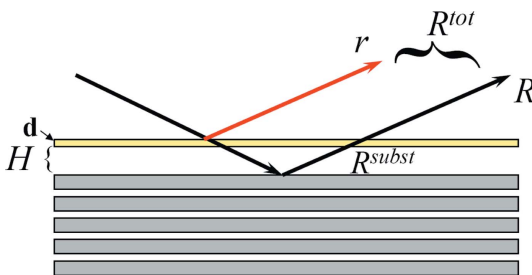[we designate $R = R^{\mathrm{substr}}\exp(iQH)$ for simplicity]. For the second term in (6), we obtain

$$\frac{[(r_{10} + R)/(1 + r_{10}R)](1 - r_{01}^2)}{\{1 + r_{01}[(r_{10} + R)/(1 + r_{10}R)]\}^2}2i\varphi^d$$

$$= \frac{(r_{10} + R)\,(1 + r_{10}R)(1 - r_{01}^2)}{(1 - r_{01}^2)^2}2i\varphi^d$$

$$= \frac{(r_{10} + R + r_{10}r_{10}R + r_{10}R^2 + 2r_{10}R - 2r_{10}R)}{(1 - r_{01}^2)}2i\varphi^d$$

$$= R\frac{(1 - r_{10})^2}{(1 - r_{01}^2)}2i\varphi^d + \frac{r_{10}}{(1 - r_{01}^2)}(1 + R)^2\,2i\varphi^d. \quad (8)$$

Taking into account the relation

$$\frac{(1 - r_{10})^2}{(1 - r_{01}^2)} = \frac{(1 + r_{01})}{(1 - r_{01})} = \frac{(1 - r_{10})}{(1 + r_{10})} = \frac{\sin\theta}{\eta}, \quad (9)$$

finally we obtain

$$R^{\mathrm{tot}} \cong R + R\frac{\sin\theta}{\eta}2ik\eta d + (1 + R)^2r^d$$

$$= R(1 + iQd) + (1 + R)^2r^d \quad (10)$$

$$\cong R^{\mathrm{substr}}\exp[iQ(H + d)] + [1 + R^{\mathrm{substr}}\exp(iQH)]^2r^d.$$

The two terms in (10) represent the reflectivity amplitude from the substrate at the top boundary of the ultrathin layer (the first term) and (the second term) from the ultrathin layer r^d, modulated by the $[1 + R^{\mathrm{substr}}\exp(iQH)]^2$ factor. If the incident wave has an amplitude equal to 1 then the term $[1 + R^{\mathrm{substr}}\exp(iQH)]$ is no other than the total field amplitude $E^{\mathrm{tot}}(H)$ at the position of the ultrathin layer, created by the interference of the incident and reflected from the substrate waves. That is, the standing wave amplitude. The expression (10) means that the reflectivity amplitude from ultrathin layer r^d placed above the reflecting substrate is modulated as $r^d \to r^{d\prime}$ by the squared standing wave amplitude $E^{\mathrm{tot}}(H)$,

$$r^{d\prime} = \left[1 + R^{\mathrm{substr}}\exp(iQH)\right]^2 r^d = \left[E^{\mathrm{tot}}(H)\right]^2 r^d. \quad (11)$$

For the first time this formula has been obtained for the explanation of the critical angle peak in the delayed nuclear resonant reflectivity (Andreeva & Lindgren, 2002, 2005), when a small resonant contribution to reflectivity is selected by time gating.

If the ultrathin layer is placed inside the multilayer structure the statement that its reflectivity amplitude is modulated by the squared standing wave amplitude is also valid. For checking this conclusion, we start from one additional boundary above the layer. The total reflectivity amplitude from the whole system is described by

$$R_1 = \frac{r_1 + R^{\mathrm{tot}}\exp(2i\varphi_0)}{1 + r_1 R^{\mathrm{tot}}\exp(2i\varphi_0)} \quad (12)$$

where $\varphi_0 = \eta_0 kd_0$, and d_0 is the distance of the new boundary from the ultrathin layer. Actually it should be $\eta_0 = \sin\theta$, because R^{tot} and r^d have been calculated for the layer in vacuum (later we can put $d_0 = 0$, $H = 0$ for a real multilayer structure). We keep the designation η_0 for the similar following calculations however. For subsequent calculations we simplify the designation in (10),

$$R^{\text{tot}} = R_0 + \Delta_0, \tag{13}$$

and take into account that Δ_0 is small enough,

$$
\begin{aligned}
R_1^{\text{out}} &= \frac{r_1 + (R_0 + \Delta_0)\exp(2i\varphi_0)}{1 + r_1(R_0 + \Delta_0)\exp(2i\varphi_0)} \\
&= \frac{r_1 + R_0\exp(2i\varphi_0) + \Delta_0\exp(2i\varphi_0)}{[1 + r_1 R_0\exp(2i\varphi_0)]\left\{1 + \frac{r_1\Delta_0}{[1 + r_1 R_0\exp(2i\varphi_0)]}\exp(2i\varphi_0)\right\}} \\
&\cong \frac{r_1 + R_0\exp(2i\varphi_0)}{[1 + r_1 R_0\exp(2i\varphi_0)]} \\
&\quad \times \left\{1 - \frac{r_1\Delta_0}{[1 + r_1 R_0\exp(2i\varphi_0)]}\exp(2i\varphi_0)\right\} \\
&\quad + \frac{\Delta_0}{[1 + r_1 R_0\exp(2i\varphi_0)]}\exp(2i\varphi_0) \\
&= \frac{r_1 + R_0\exp(2i\varphi_0)}{[1 + r_1 R_0\exp(2i\varphi_0)]} \\
&\quad + \left\{\Delta_0\exp(2i\varphi_0)\right. \\
&\quad \left. \times \frac{1 + r_1 R_0\exp(2i\varphi_0) - r_1^2 - r_1 R_0\exp(2i\varphi_0)}{[1 + r_1 R_0\exp(2i\varphi_0)]^2}\right\} \\
&= \frac{r_1 + R_0\exp(2i\varphi_0)}{[1 + r_1 R_0\exp(2i\varphi_0)]} \\
&\quad + \Delta_0\exp(2i\varphi_0)\frac{(1 - r_1^2)}{[1 + r_1 R_0\exp(2i\varphi_0)]^2}. \tag{14}
\end{aligned}
$$

For the next boundary we use the designation

$$
\begin{aligned}
R_1^{\text{out}} &= \frac{r_1 + R_0\exp(2i\varphi_0)}{[1 + r_1 R_0\exp(2i\varphi_0)]} \\
&\quad + \Delta_0\exp(2i\varphi_0)\frac{(1 - r_1^2)}{[1 + r_1 R_0\exp(2i\varphi_0)]^2} \\
&= R_1 + \Delta_1, \tag{15}
\end{aligned}
$$

and repeat the same kind of calculations as in (14) with the renumbered indices. So the calculation shows that, for each additional j boundary above the ultrathin layer [we numerate the boundaries in opposite order than in the recursive expression (1)], the expression (11) is supplemented with the factor

$$\exp(2i\varphi_{j-1})\frac{(1 - r_j^2)}{[1 + r_j R_{j-1}\exp(2i\varphi_{j-1})]^2}, \tag{16}$$

with the exception of the zero artificial vacuum layer, for which we put $\exp(2i\varphi_{j-1}) = 1$.

Finally, we obtain

$$r^{d'}(z) = T(z)\,T'(z)\,[1 + R^{\text{below}}(z)]^2\,r^d = E_{\text{tot}}^2(z)\,r^d, \tag{17}$$

where the functions $T(z)T'(z)$ describe the transformations of the transmitted and outgoing waves during multiple reflections at all boundaries in the upper part of the multilayer,

$$
\begin{aligned}
T(z)T'(z) &= \exp[2i(\varphi_1 + \ldots + \varphi_{j-1})] \tag{18}\\
&\quad \times \frac{(1 - r_1^2)(1 - r_2^2)\ldots(1 - r_j^2)}{(1 + r_1 R_0)^2[1 + r_2 R_1\exp(2i\varphi_1)]^2\ldots[1 + r_j R_{j-1}\exp(2i\varphi_{j-1})]^2}
\end{aligned}
$$

(j numerates the boundaries above the layer). It should be mentioned that r^d corresponds to the reflectivity amplitude from an ultrathin layer in vacuum (3), so the vacuum spacers below and upper the ultrathin layer should be considered, but due to their artificial nature the thicknesses H in (11) and d_0 (in φ_0) in (12), (18) must be put as 0.

Taking into account the well known Fresnel relations at each boundary,

$$
\begin{aligned}
1 - r_i^2 &= (1 - r_i)(1 + r_i) = \left(1 - \frac{\eta_i - \eta_{i-1}}{\eta_i + \eta_{i-1}}\right)\left(1 - \frac{\eta_{i-1} - \eta_i}{\eta_i + \eta_{i-1i}}\right) \\
&= t_i t_i', \tag{19}\\
t_i &= \frac{2\eta_i}{\eta_i + \eta_{i-1}}, \qquad t_i' = \frac{2\eta_{i-1}}{\eta_i + \eta_{i-1}},
\end{aligned}
$$

two separate functions (each one for the waves in the forward and backward directions, respectively) can be extracted from (18),

$$
\begin{aligned}
T(z) &= \exp[i(\varphi_1 + \varphi_2 + \ldots + \varphi_{j-1})] \tag{20}\\
&\quad \times \frac{(1 + r_1)(1 + r_2)\ldots(1 + r_{j-1})}{(1 + r_1 R_0)[1 + r_2 R_1\exp(2i\varphi_1)]\ldots[1 + r_j R_{j-1}\exp(2i\varphi_{j-1})]}
\end{aligned}
$$

and

$$T'(z) = T(z)\frac{\eta_{j-1}}{\eta_0}. \tag{21}$$

Omitting the multiple scatterings in the kinematical approximation, these functions are simplified to the well known expression describing the phase incursion for the transmitted and outgoing waves in the upper part of the multilayer,

$$T(z)T'(z) = \exp\left(iQz + \frac{2\pi}{\lambda\sin\vartheta}\sum_{m=1}^{j-1}\chi_m\,d_m\right). \tag{22}$$

The multistep function for calculation of the field amplitude at depth z in (18) is not convenient for the cases of a large amount of layers. The propagation matrix method provides a much more effective way for such calculations. The appropriate formulas for the reflectivity by an ultrathin layer inside a multilayer are given in Appendix A.

The intensity of the total reflectivity includes the squared module of both terms in (10) or (15)) and the interference term. The most interesting case happens when in the experiment it is possible to select only the second term $r^{d'}$. It takes place, for example, in the time domain nuclear resonant reflectivity when the resonance scattering gives the delayed signal (Toellner et al., 1995; Baron et al., 1994). In this case the time gating separates the nuclear resonant response of nuclei, placed at some depth, i.e. only the second term (10) should be considered (Andreeva & Lindgren, 2002, 2005). In this article we consider another way to separate the small resonant contribution from total reflectivity, namely by the polarization analysis of reflected radiation.

3. Anisotropic ultrathin layer

The reflectivity amplitude from an ultrathin anisotropic layer can be considered by means of the propagation matrix. In the anisotropic case the propagation matrix is a 4×4 matrix and it describes the variation of the two-dimential tangential vectors

$$\mathbf{H}_t = -\mathbf{q} \times \mathbf{q} \times \mathbf{H} = \begin{pmatrix} H_x \\ H_y \end{pmatrix} \quad \text{and} \quad \mathbf{q} \times \mathbf{E} = \begin{pmatrix} -E_y \\ E_x \end{pmatrix}$$

of the plane electromagnetic wave $\exp(ikr - i\omega t)$ in a layered medium (the x axis is chosen perpendicular to the reflection plane, the y axis in the reflection plane – Fig. 2),

$$\frac{\mathrm{d}}{\mathrm{d}z}\begin{pmatrix} \mathbf{H}_t \\ \mathbf{q} \times \mathbf{E} \end{pmatrix} = ik\hat{M}\begin{pmatrix} \mathbf{H}_t \\ \mathbf{q} \times \mathbf{E} \end{pmatrix}$$

or

$$\frac{\mathrm{d}}{\mathrm{d}z}\begin{pmatrix} H_x(z) \\ H_y(z) \\ -E_y(z) \\ E_x(z) \end{pmatrix} = ik\hat{M}(z)\begin{pmatrix} H_x(z) \\ H_y(z) \\ -E_y(z) \\ E_x(z) \end{pmatrix}. \tag{23}$$

In the general case the matrix $\hat{M}(z)$ has been calculated [see the textbook by Azzam & Bashara (1977)] by the coordinate method, and by the covariant tensor method by Borzdov *et al.* (1976) and Barkovskii *et al.* (1983). If the material equations include just the tensor of the electric susceptibility $\hat{\chi}$ [$\mathbf{D} = \hat{\varepsilon}\mathbf{E} = (1 + \hat{\chi})\mathbf{E}$, $\mathbf{B} = \mathbf{H}$], then $\hat{M}(z)$ is presented in the following form (Borzdov *et al.*, 1976; Andreeva & Smekhova, 2006),

$$\hat{M} = \begin{pmatrix} \frac{1}{\varepsilon_q}\mathbf{q}^{\times}\hat{\varepsilon}\mathbf{q}\circ\mathbf{a} & \frac{1}{\varepsilon_q}\hat{I}\,\bar{\hat{\varepsilon}}\,\hat{I} - \mathbf{b}\circ\mathbf{b} \\ \hat{I} - \frac{1}{\varepsilon_q}\mathbf{a}\circ\mathbf{a} & -\frac{1}{\varepsilon_q}\mathbf{a}\circ\mathbf{q}\,\hat{\varepsilon}\,\mathbf{q}^{\times} \end{pmatrix}$$

$$= \begin{pmatrix} -\frac{\chi_{yz}}{1+\chi_{zz}}\cos\theta & 0 & 1+\chi_{yy}-\frac{\chi_{zy}\chi_{yz}}{1+\chi_{zz}} & \frac{\chi_{yz}\chi_{zx}}{1+\chi_{zz}}-\chi_{yx} \\ \frac{\chi_{xz}}{1+\chi_{zz}}\cos\theta & 0 & \frac{\chi_{zy}\chi_{xz}}{1+\chi_{zz}}-\chi_{xy} & \chi_{xx}-\frac{\chi_{zx}\chi_{xz}}{1+\chi_{zz}}+\sin^2\theta \\ 1-\frac{\cos^2\theta}{1+\chi_{zz}} & 0 & -\frac{\chi_{zy}}{1+\chi_{zz}}\cos\theta & \frac{\chi_{zx}}{1+\chi_{zz}}\cos\theta \\ 0 & 1 & 0 & 0 \end{pmatrix}$$

$$\simeq \begin{pmatrix} -\chi_{yz}\cos\theta & 0 & 1+\chi_{yy} & -\chi_{yx} \\ \chi_{xz}\cos\theta & 0 & -\chi_{xy} & \sin^2\theta+\chi_{xx} \\ \frac{\sin^2\theta+\chi_{zz}}{1+\chi_{zz}} & 0 & -\chi_{zy}\cos\theta & \chi_{zx}\cos\theta \\ 0 & 1 & 0 & 0 \end{pmatrix}, \tag{24}$$

using the following notations: $\mathbf{b}$ is the unchanged tangential components of all wavevectors in units of ω/c, $\mathbf{a} = \mathbf{b} \times \mathbf{q}$, $|\mathbf{b}| = |\mathbf{a}| = \cos\theta$, $\hat{I} = 1 - \mathbf{q}\circ\mathbf{q} = -(\mathbf{q}^{\times})^2$ is the projective tensor, $\mathbf{q}^{\times}$ is a dual tensor performing the vector product, $\varepsilon_q = \mathbf{q}\,\hat{\varepsilon}\,\mathbf{q}$, $\bar{\hat{\varepsilon}} = (\mathbf{q}^{\times}\hat{\varepsilon}\mathbf{q}\circ\mathbf{q}\,\hat{\varepsilon}\,\mathbf{q}^{\times} - \mathbf{q}^{\times}\hat{\varepsilon}\,\mathbf{q}\mathbf{q}\,\hat{\varepsilon}\,\mathbf{q})$ is the reciprocal of the transposed matrix $\hat{\varepsilon}$, and the sign $\circ$ designates the operation of the outer product of the vectors.

The integral propagation matrix $\hat{L}(d)$ for an ultrathin layer of thickness d and $\hat{\chi}(z) = \text{const}$ can be easily calculated by the expansion of the matrix exponential up to the first order of kd,
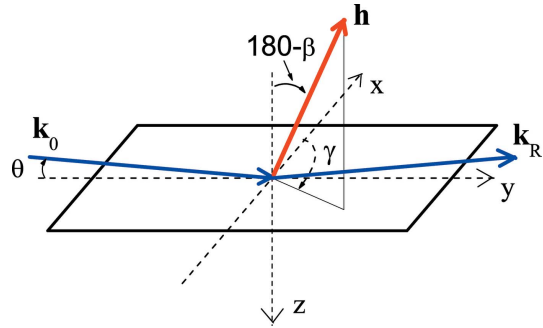

Figure 2
The coordinate system used. $\mathbf{k}_0$ and $\mathbf{k}_R$ are the wavevectors of the incident and reflected plane waves, β and γ are the polar and azimuth angles for the magnetization unit vector $\mathbf{h}$.

$$\hat{L}(d) = \exp(ikd\hat{M}) = \begin{pmatrix} \hat{l}_1 & \hat{l}_2 \\ \hat{l}_3 & \hat{l}_4 \end{pmatrix} \simeq 1 + ikd\hat{M} \simeq \tag{25}$$

$$\begin{pmatrix} 1 - ikd\,\chi_{yz}\cos\theta & 0 & ikd\,(1+\chi_{yy}) & -ikd\,\chi_{yx} \\ ikd\,\chi_{xz}\cos\theta & 1 & -ikd\,\chi_{xy} & ikd\,(\sin^2\theta+\chi_{xx}) \\ ikd\,\frac{\sin^2\theta+\chi_{zz}}{1+\chi_{zz}} & 0 & 1-ikd\,\chi_{zy}\cos\theta & ikd\,\chi_{zx}\cos\theta \\ 0 & ikd & 0 & 1 \end{pmatrix}.$$

It is convenient to dismember the 4×4 matrix into 2×2 blocks $\hat{l}_j$, $j = 1, \ldots 4$.

The boundary task with the integral propagation matrix is presented by a system of four equations (for the two two-dimensional vectors),

$$\begin{pmatrix} \mathbf{H}_t^T \\ \mathbf{q} \times \mathbf{E}^T \end{pmatrix} = \begin{pmatrix} \hat{l}_1 & \hat{l}_2 \\ \hat{l}_3 & \hat{l}_4 \end{pmatrix}\begin{pmatrix} \mathbf{H}_t^0 + \mathbf{H}_t^R \\ \mathbf{q} \times \mathbf{E}^0 + \mathbf{q} \times E^R \end{pmatrix}. \tag{26}$$

We define the reflectivity amplitude $\hat{p}$ for the tangential components of the magnetic field of radiation by the relation

$$\mathbf{H}_t^R = \hat{p}\,\mathbf{H}_t^0 \tag{27}$$

($\hat{p}$ is now a 2×2 matrix), and introduce the 2×2 matrices $\hat{\gamma}^{0,R,T}$ supplying the link between the tangential vectors $\mathbf{H}_t$ and $\mathbf{q} \times \mathbf{E}$ in the incident, reflected and transmitted waves (superscripts 0, R and T, respectively),

$$\mathbf{q} \times \mathbf{E}^{0,R,T} = \hat{\gamma}^{0,R,T}\mathbf{H}_t^{0,R,T}. \tag{28}$$

Then the solution of (26) is presented by the following expression (Borzdov *et al.*, 1976),

$$\hat{p} = \left[\hat{\gamma}^T(\hat{l}_1 + \hat{l}_2\hat{\gamma}^R) - (\hat{l}_3 + \hat{l}_4\hat{\gamma}^R)\right]^{-1}$$
$$\times \left[(\hat{l}_3 + \hat{l}_4\hat{\gamma}^0) - \hat{\gamma}^T(\hat{l}_1 + \hat{l}_2\hat{\gamma}^0)\right]. \tag{29}$$

If an ultrathin layer is situated in a vacuum, the matrices $\hat{\gamma}^{0,R,T}$ have the very simple form

$$\hat{\gamma}^{0,R,T} = \pm\begin{pmatrix} \sin\theta & 0 \\ 0 & 1/\sin\theta \end{pmatrix}, \tag{30}$$

where the sign $\pm$ refers to the wves in the direct (0, T) and opposite (R) directions.

Calculation of the 'numerator' in (29) in the first approximation gives

$$(\hat{l}_3 + \hat{l}_4\hat{\gamma}^0) - \hat{\gamma}^T(\hat{l}_1 + \hat{l}_2\hat{\gamma}^0)$$

$$= \begin{pmatrix} ikd\,[(\sin^2\theta + \chi_{zz})/(1+\chi_{zz})] & 0 \\ 0 & ikd \end{pmatrix}$$

$$+ \begin{pmatrix} 1 - ikd\,\chi_{zy}\cos\theta & ikd\,\chi_{zx}\cos\theta \\ 0 & 1 \end{pmatrix}\begin{pmatrix} \sin\theta & 0 \\ 0 & 1/\sin\theta \end{pmatrix}$$

$$- \begin{pmatrix} \sin\theta & 0 \\ 0 & 1/\sin\theta \end{pmatrix}\left[\begin{pmatrix} 1 - ikd\,\chi_{yz}\cos\theta & 0 \\ ikd\,\chi_{xz}\cos\theta & 1 \end{pmatrix}\right.$$

$$\left. + \begin{pmatrix} ikd\,(1+\chi_{yy}) & -ikd\,\chi_{yx} \\ -ikd\,\chi_{xy} & ikd\,(\sin^2\theta + \chi_{xx}) \end{pmatrix}\begin{pmatrix} \sin\theta & 0 \\ 0 & 1/\sin\theta \end{pmatrix}\right]$$

$$= ikd \begin{pmatrix} \chi_{zz}\cos^2\theta - \chi_{yy}\sin^2\theta & (1/\sin\theta)(\chi_{zx}\cos\theta \\ + (\chi_{yz} - \chi_{zy})\cos\theta\sin\theta & + \chi_{yx}\sin\theta) \\ (-1/\sin\theta)(\chi_{xz}\cos\theta - \chi_{xy}\sin\theta) & -\chi_{xx}/\sin^2\theta \end{pmatrix}$$

$$\tag{31}$$

The 'denominator' in (29) in the first approximation can be simplified to

$$[\hat{\gamma}^T(\hat{l}_1 + \hat{l}_2\hat{\gamma}^R) - (\hat{l}_3 + \hat{l}_4\hat{\gamma}^R)]$$

$$= \begin{pmatrix} 1 - ikd\,\chi_{zy}\cos\theta & ikd\,\chi_{zx}\cos\theta \\ 0 & 1 \end{pmatrix}\begin{pmatrix} \sin\theta & 0 \\ 0 & 1/\sin\theta \end{pmatrix}$$

$$- \begin{pmatrix} ikd\,[(\sin^2\theta + \chi_{zz})/(1+\chi_{zz})] & 0 \\ 0 & ikd \end{pmatrix}$$

$$+ \begin{pmatrix} \sin\theta & 0 \\ 0 & 1/\sin\theta \end{pmatrix}\left[\begin{pmatrix} 1 - ikd\,\chi_{yz}\cos\theta & 0 \\ ikd\,\chi_{xz}\cos\theta & 1 \end{pmatrix}\right.$$

$$\left. - \begin{pmatrix} ikd\,(1+\chi_{yy}) & -ikd\,\chi_{yx} \\ -ikd\,\chi_{xy} & ikd\,(\sin^2\theta + \chi_{xx}) \end{pmatrix}\begin{pmatrix} \sin\theta & 0 \\ 0 & 1/\sin\theta \end{pmatrix}\right]$$

$$\cong \begin{pmatrix} 2\sin\theta & 0 \\ 0 & 2/\sin\theta \end{pmatrix}, \tag{32}$$

and the inverse matrix is easily calculated

$$\begin{pmatrix} 2\sin\theta & 0 \\ 0 & 2/\sin\theta \end{pmatrix}^{-1} = \frac{1}{4}\begin{pmatrix} 2/\sin\theta & 0 \\ 0 & 2\sin\theta \end{pmatrix}. \tag{33}$$

Finally, we obtain

$$\hat{p} = \frac{ikd}{2}\begin{pmatrix} 1/\sin\theta & 0 \\ 0 & \sin\theta \end{pmatrix} \tag{34}$$

$$\times \begin{pmatrix} \chi_{zz}\cos^2\theta - \chi_{yy}\sin^2\theta & (1/\sin\theta)(\chi_{zx}\cos\theta \\ + (\chi_{yz} - \chi_{zy})\cos\theta\sin\theta & + \chi_{yx}\sin\theta) \\ (-1/\sin\theta)(\chi_{xz}\cos\theta - \chi_{xy}\sin\theta) & -\chi_{xx}/\sin^2\theta \end{pmatrix}$$

$$= \frac{ikd}{2\sin\theta}\begin{pmatrix} \chi_{zz}\cos^2\theta - \chi_{yy}\sin^2\theta & (1/\sin\theta)(\chi_{zx}\cos\theta \\ + (\chi_{yz} - \chi_{zy})\cos\theta\sin\theta & + \chi_{yx}\sin\theta) \\ -\sin\theta(\chi_{xz}\cos\theta & \\ -\chi_{xy}\sin\theta) & -\chi_{xx} \end{pmatrix}.$$

Instead of (27) it is reasonable to have the reflectivity matrix for the electric field of radiation $\hat{r}$ and present it in the σ- and π-polarization basis. If in the outward medium $\chi_0 = 0$, the conversion from $\hat{p}$ to $\hat{r}$ is simple,

$$\hat{r} = \begin{pmatrix} r_{\sigma\to\sigma'} & r_{\pi\to\sigma'} \\ r_{\sigma\to\pi'} & r_{\pi\to\pi'} \end{pmatrix} = \begin{pmatrix} -p_{22} & p_{21}/\sin\theta \\ -p_{12}\sin\theta & p_{11} \end{pmatrix}. \tag{35}$$

The reflectivity matrix amplitude for a single ultrathin layer takes the following expression,

$$\hat{r}^d \cong \frac{ikd}{2\sin\theta}\hat{\chi}^\perp, \tag{36}$$

where the transverse (to the propagation directions) susceptibility tensor $\hat{\chi}^\perp$ in σ- and π-polarization basis is introduced,

$$\hat{\chi}^\perp = \begin{pmatrix} \chi_{\sigma\to\sigma'} & \chi_{\pi\to\sigma'} \\ \chi_{\sigma\to\pi'} & \chi_{\pi\to\pi'} \end{pmatrix} \tag{37}$$

$$= \begin{pmatrix} \chi_{xx} & \chi_{xy}\sin\theta - \chi_{xz}\cos\theta \\ -\chi_{yx}\sin\theta - \chi_{zx}\cos\theta & \chi_{zz}\cos^2\theta - \chi_{yy}\sin^2\theta \\ & + \cos\theta\sin\theta(\chi_{yz} - \chi_{zy}) \end{pmatrix}.$$

4. Magnetic contribution from a single layer

The magnetic contributions of the circular $\Delta\chi_m$ and linear $\Delta\chi_l$ dichroism to the susceptibility χ_0 in the case of the dipole resonance transitions can be presented in the following form (Stepanov & Sinha, 2000),

$$\hat{\chi} = \chi_0 + i\Delta\chi_m\mathbf{h}^\times + \Delta\chi_l\mathbf{h}\circ\mathbf{h}, \tag{38}$$

where $\mathbf{h}$ is the unit vector in the direction of magnetization, $\mathbf{h}^\times$ is the dual tensor, describing the operation of the vector product, and the sign $\circ$ designates the operation of the outer product of the vectors.

In the chosen coordinate system (Fig. 2) the magnetization unit vector $\mathbf{h}$ has the following components,

$$\mathbf{h} = (\sin\beta\cos\gamma, \sin\beta\sin\gamma, \cos\beta). \tag{39}$$

Typically, $\Delta\chi_l$ is much smaller than $\Delta\chi_m$, so neglecting $\Delta\chi_l$ we have

$$\hat{\chi} = \chi_0 \begin{pmatrix} 1 & 0 & 0 \\ 0 & 1 & 0 \\ 0 & 0 & 1 \end{pmatrix} \tag{40}$$

$$+ \begin{pmatrix} 0 & -i\Delta\chi_m\cos\beta & \begin{matrix} i\Delta\chi_m \\ \times\sin\beta\sin\gamma \end{matrix} \\ i\Delta\chi_m\cos\beta & 0 & \begin{matrix} -i\Delta\chi_m \\ \times\sin\beta\cos\gamma \end{matrix} \\ \begin{matrix} -i\Delta\chi_m \\ \times\sin\beta\sin\gamma \end{matrix} & i\Delta\chi_m\sin\beta\cos\gamma & 0 \end{pmatrix}.$$

Supposing that the magnetization in the ultrathin layer is arranged in the surface plane and along the grazing beam (L-MOKE geometry, $\beta = 90°$ and $\gamma = 90°$), we obtain

$$\hat{\chi} = \begin{pmatrix} \chi_0 & 0 & i\Delta\chi_m \\ 0 & \chi_0 & 0 \\ -i\Delta\chi_m & 0 & \chi_0 \end{pmatrix}, \tag{41}$$

and from (36) and (37)

$$\hat{r}^d \cong \frac{ikd}{2\sin\theta}\begin{pmatrix} \chi_0 & -i\Delta\chi_m\cos\theta \\ i\Delta\chi_m\cos\theta & \chi_0\cos2\theta \end{pmatrix}. \tag{42}$$

Thus, for a σ-polarized incident wave, the amplitude of which is represented as

$$\begin{pmatrix} 1 \\ 0 \end{pmatrix},$$

we have the reflectivity amplitude of the same σ-polarization,

$$r_{\sigma\to\sigma'} = \frac{ikd}{2\sin\theta}\chi_0 \tag{43}$$

and the reflectivity amplitude with the rotated π'-polarization,

$$r_{\sigma\to\pi'} = \frac{-kd}{2\sin\theta}\Delta\chi_m\cos\theta. \tag{44}$$

Making use of (10), the reflectivity from such a magnetic ultrathin layer placed under the reflecting substrate can be written

$$\left|R^{\mathrm{tot}}\right|^2 \simeq \left|R^{\mathrm{substr}}\exp[iQ(H+d)] + [E^{\mathrm{tot}}(H)]^2 r_{\sigma\to\sigma'}\right|^2 + \left|[E^{\mathrm{tot}}(H)]^2 r_{\sigma\to\pi'}\right|^2, \tag{45}$$

where $E^{\mathrm{tot}}(H) = 1 + R^{\mathrm{substr}}\exp(iQH)$ is the total radiation field amplitude at the position of the magnetic layer, and H is the distance of this layer from the substrate. The expression (45) contains two terms: the first one presents the reflectivity with the same polarization as the incident wave and the second one corresponds to the rotated π-polarization in the reflectivity. The second part of the total reflectivity has the rotated π-polarization which has a pure magnetic scattering origin,

$$\left|R_{\sigma\to\pi'}\right|^2 = \left|[E_{\mathrm{tot}}(H)]^2\frac{kd\cos\theta}{2\sin\theta}\Delta\chi_m\right|^2. \tag{46}$$

In the general case of the arbitrary magnetization direction the reflectivity with rotated polarization $|R_{\sigma\to\pi}|^2$ takes the form

$$\left|R_{\sigma\to\pi'}\right|^2 = \left|\frac{kd}{2\sin\theta}[E_{\mathrm{tot}}(H)]^2\chi_{\sigma\to\pi'}\right|^2 \tag{47}$$

$$= \left|\frac{kd}{2\sin\theta}[E_{\mathrm{tot}}(H)]^2(-\chi_{yx}\sin\theta - \chi_{zx}\cos\theta)\right|^2.$$

Fig. 3 demonstrates the angular dependence of this dichroic component $|R_{\sigma\to\pi'}|^2$ for different distance H of this thin layer from the substrate. The calculations are performed for the L_2-edge of gadolinium ($E_{\mathrm{ph}} = 7930$ eV, $\lambda = 0.1563$ nm). For a Gd layer of thickness 0.1 nm we put $\chi_0 = (-31.0 + i10.0) \times 10^{-6}$ and $\Delta\chi_m = (-0.1 - i0.23) \times 10^{-6}$ [the data are taken from Sorg $et~al.$ (2007)], for the Si substrate $\chi_0 = (-15.6 + i0.37) \times 10^{-6}$ (http://henke.lbl.gov/optical_constants/getdb2.html).
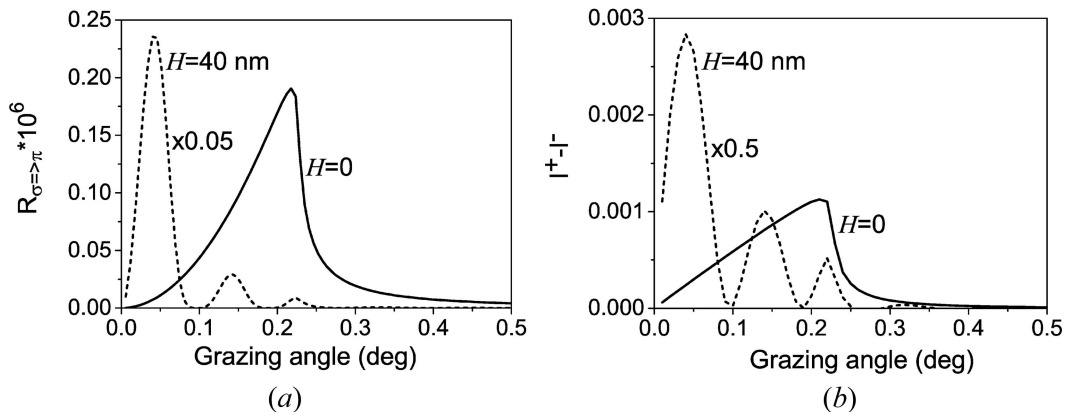
Figure 3
Angular dependences of the reflectivity with the rotated polarization (a) and the reflectivity difference ($I_+ - I_-$) (b), calculated for the ultrathin magnetic layer, placed at different distances from the Si substrate and magnetized along the beam. It is interesting to note that the peculiarities near the critical angle disappeared in the asymmetry angular dependence ($I_+ - I_-$)/($I_+ + I_-$) due to the strong variations of the denominator ($I_+ + I_-$) in this region.

 489

The obtained angular dependencies (Fig. 3) are similar to the ones presented in the paper by Bedzyk *et al.* (1989) devoted to the standing wave influence on the fluorescent yield from heavy atoms incorporated into Langmuir layers. However, the contrast of oscillations in the calculated dependencies of the reflectivity with the rotated polarization is more pronounced due to the squared standing wave amplitude. This should have a consequence in the enhanced surface sensitivity. It is important that the curves in Fig. 3, calculated by the simple expression (46) and by the exact theory of the magnetic reflectivity with 4×4 propagation matrices, are identical.

It is reasonable to compare two possible kinds of measurements. The results presented in Fig. 3(a) need linear polarization of the incident radiation and polarization analysis of the reflected intensity. Commonly for magnetic investigations by the reflectivity method (XRMR), the two circular polarizations of the incident radiation are used and the asymmetry of the two reflectivity curves $(I_+ - I_-)/(I_+ + I_-)$ is analyzed. Supposing that the total reflectivity amplitude is a matrix in σ- and π-polarization orts,

$$\hat{R}^{\text{tot}} = \begin{bmatrix} R_{\sigma\sigma} & R_{\sigma\pi} \\ R_{\pi\sigma} & R_{\pi\pi} \end{bmatrix}, \qquad (48)$$

then the intensity of the reflected radiation for the right and left circular polarization I_+ and I_- can be calculated according to the expressions

$$I_+ = \frac{1}{2} \left(\left| R_{\sigma\sigma} + iR_{\sigma\pi} \right|^2 + \left| R_{\pi\sigma} + iR_{\pi\pi} \right|^2 \right) \qquad (49)$$
$$= \frac{1}{2} \left\{ \left| R_{\sigma\sigma} \right|^2 + \left| R_{\sigma\pi} \right|^2 + 2\left(\text{Re}R_{\sigma\pi}\text{Im}R_{\sigma\sigma} - \text{Re}R_{\sigma\sigma}\text{Im}R_{\sigma\pi} \right) \right. $$
$$\left. + \left| R_{\pi\sigma} \right|^2 + \left| R_{\pi\pi} \right|^2 + 2\left(\text{Re}R_{\pi\pi}\text{Im}R_{\pi\sigma} - \text{Re}R_{\pi\sigma}\text{Im}R_{\pi\pi} \right) \right\},$$

$$I_- = \frac{1}{2} \left(\left| R_{\sigma\sigma} - iR_{\sigma\pi} \right|^2 + \left| R_{\pi\sigma} - iR_{\pi\pi} \right|^2 \right) \qquad (50)$$
$$= \frac{1}{2} \left\{ \left| R_{\sigma\sigma} \right|^2 + \left| R_{\sigma\pi} \right|^2 - 2\left(\text{Re}R_{\sigma\pi}\text{Im}R_{\sigma\sigma} - \text{Re}R_{\sigma\sigma}\text{Im}R_{\sigma\pi} \right) \right. $$
$$\left. + \left| R_{\pi\sigma} \right|^2 + \left| R_{\pi\pi} \right|^2 - 2\left(\text{Re}R_{\pi\pi}\text{Im}R_{\pi\sigma} - \text{Re}R_{\pi\sigma}\text{Im}R_{\pi\pi} \right) \right\},$$

and the difference in the reflectivity takes the form

$$(I_+ - I_-) = 2\left(\text{Re}R_{\pi\pi}\text{Im}R_{\pi\sigma} - \text{Re}R_{\sigma\sigma}\text{Im}R_{\sigma\pi} \right. $$
$$\left. + \text{Im}R_{\sigma\sigma}\text{Re}R_{\sigma\pi} - \text{Im}R_{\pi\pi}\text{Re}R_{\pi\sigma} \right). \qquad (51)$$

From (51) it follows that the reflectivity amplitudes with the rotated polarization, which have a purely magnetic scattering origin and are typically very small, are enhanced in this XRMR method by the much higher $R_{\sigma\sigma}$ and $R_{\pi\pi}$ reflectivity amplitudes of scattering without polarization change. This circumstance makes the measurements of the magnetic scattering easier, but on the other hand it essentially complicates the data treatment directed to the extraction of the magnetic scattering information. The expression (51) disproves the assertion of Höchst *et al.* (1996, 1997) about a pure magnetic origin of the measured asymmetry ratio. Note that the selection of the purely magnetic scattering part had been carried

out by Mertins *et al.* (2002) by a complicated combination of different kinds of measurements (L-MOKE, T-MOKE and Faraday rotation) on a ferromagnetic Fe/C multilayer at the Fe-2*p* absorption edge.

It is clear that using the selection of the reflectivity with rotated π'-polarization directly gives the purely magnetic scattering part separately from the dominant $R_{\sigma\sigma}$ and $R_{\pi\pi}$ reflectivity.

The obtained formulas (47) and (51) suggest the most effective way for the calculation of the magnetic addition to the reflectivity instead of the very time-consuming algorithm based on the 4×4 propagation matrices.

5. Magnetic reflectivity from the whole magnetic structure

The magnetic contribution to the scattering is typically small enough and it does not influence the total radiation field inside the whole sample; therefore we can suppose that the magnetic scattering from different layers is independent of each other. In this case the magnetic scattering amplitudes with proper phases can be summarized as is done in the kinematical theory of reflectivity. The analogous procedure has been used by Ott *et al.* (2006). However, in contrast to that paper we will take into account the influence of the total radiation field $E(\theta, z)$ (standing waves) at different depths z on the magnetic scattering, as follows from (11), (17) and (46). So, for calculation of the reflectivity with the rotated polarization we suggest the following expression, which is actually the generalized kinematical approximation,

$$I_{\sigma \to \pi'}(\theta) = \left| \frac{\pi}{\lambda \sin\theta} \int \chi^{\sigma \to \pi'}(z) \, E_\sigma^2(\theta, z) \, \mathrm{d}z \right|^2, \qquad (52)$$

where $\chi^{\sigma \to \pi'}$ is the magnetic off-diagonal element of the transverse susceptibility tensor $\hat{\chi}^\perp$ (37). Direct calculations performed using this formula demonstrate a surprisingly perfect agreement with the calculations by the exact matrix theory for all angles of incidence including the region of total external reflection (Figs. 4 and 5).

The off-diagonal elements of the reflectivity matrix amplitude, needed for the asymmetry ratio calculations by expression (51), can be obtained similarly to (52),

$$R_{\sigma\pi(\pi\sigma)}(\theta) = \frac{i\pi}{\lambda \sin\theta} \int \chi^{\sigma\pi(\pi\sigma)}(z) \, E_{\sigma(\pi)}^2(\theta, z) \, \mathrm{d}z. \qquad (53)$$

The diagonal elements of the amplitude reflectivity matrix $R_{\sigma\sigma}$ and $R_{\pi\pi}$ in (51) can be calculated ignoring magnetic contributions by the simple Parratt algorithm, for example. Figs. 4 and 5 show that such a way for the asymmetry ratio calculations also gives results identical to the exact calculations.

The calculated depth-distribution of the total field (more precisely the squared standing waves) drawn in Fig. 4 is independent of the type of magnetization ordering in the multilayer and it can be used as the basis for the calculations of the rotated reflectivity and asymmetry ratio by (52), (51) and (53) for ferromagnetic, antiferromagnetic and spiral interlayer
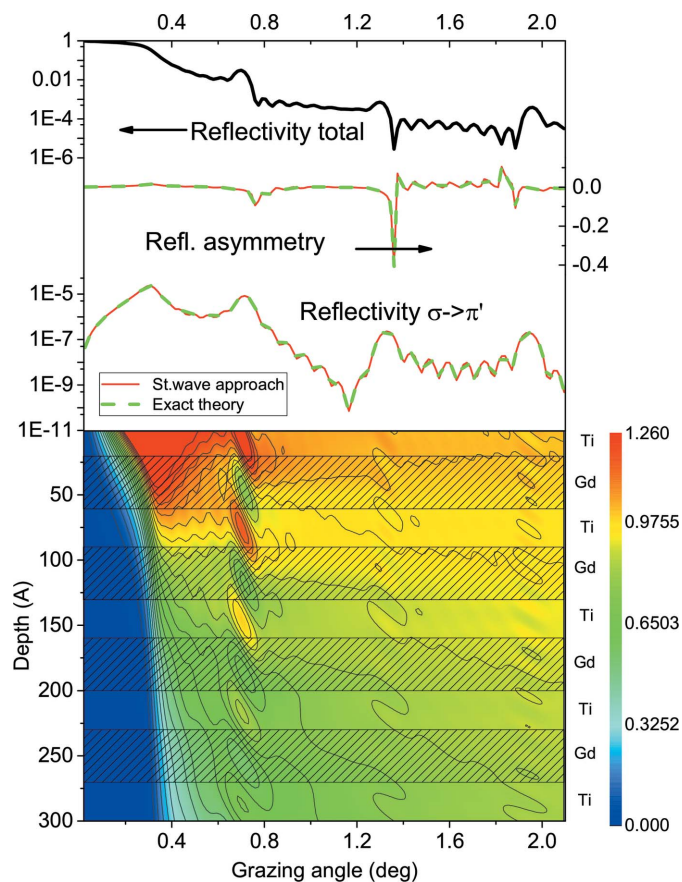
Figure 4
Squared standing waves $|E_\sigma^2(\theta, z)|^2$ inside a [Ti(3 nm)/Gd(4 nm)]$_8$ multi-layer at different grazing angles (bottom part), the rotated reflectivity $I_{\sigma \to \pi'}$, the asymmetry ratio $A = (I_+ - I_-)/(I_+ + I_-)$ and the total reflectivity (top graphs). $E_\sigma(\theta, z)$ is normalized to the amplitude of the incident wave $E_0 = 1$. Calculations for $E_{ph} = 7930$ eV and with the same parameters of Gd susceptibility as in Fig. 3. Multilayer magnetization is supposed along the beam (L-MOKE geometry). The magnetic contributions to the reflectivity originate only from Gd layers (hatched); therefore the integration in (52) and (53) concerns only this hatched regions. Thin (red) lines show $A(\theta)$ and $I_{\sigma \to \pi'}(\theta)$ calculated by the exact theory [program pack by Andreeva & Repchenko (2017)], thick dashed (green) lines show the results of $A(\theta)$ and $I_{\sigma \to \pi'}(\theta)$ calculations obtained by (51), (53) and (52), respectively.

coupling between Gd layers. The calculation results for these cases are shown in Fig. 5.

Figs. 4 and 5 show that both the angular curves for the asymmetry ratio and for the reflectivity with rotated polarization characterize the peculiarities of the magnetic ordering by specific maxima at Bragg angles or by the magnetic satellites, but the shapes of the two dependences are rather different. Therefore, it is clear that the measurements of the rotated polarization are very helpful for investigations of the complicated magnetic structures.

The significance of the expression (52) is stipulated by two aspects. Firstly, it allows us to calculate the magnetic reflectivity much faster without 4×4 propagation matrices, because the most complicated part of the standing wave calculations can be performed by the scalar theory of reflectivity (*e.g.* by the Parratt algorithm). It essentially speeds up the model

calculations and fit procedure. Secondly, the interpretation of the reflectivity with the rotated polarization based on the squared standing waves explains the exclusive depth selectivity of the measurements using the polarization analysis.

6. Experimental test

The most important evidence for the influence of the standing wave on the magnetic reflectivity with rotated polarization is the observation of a peak near the critical angle of the total reflection in the angular dependence.

The first experimental test of this peculiarity on the angular curve of reflectivity with the rotated polarization was carried out for Ti(10 nm)/Gd$_{0.23}$Co$_{0.77}$(250 nm)/Ti(10 nm) film at the L_2-edge of Gd (Andreeva *et al.*, 2018a). The sample has the compensation temperature of $T_{comp} \simeq 433$ K for Co and Gd subsystem magnetizations (Svalov *et al.*, 2016), so at room temperature the Gd atoms should possess magnetic moments. The measurements were performed at the Kurchatov Center for Synchrotron Radiation and Nanotechnology (KCSRN). The sample was placed on a piece of permanent magnet in order to magnetize it along the beam. The analysis of the polarization state of the reflected radiation was performed by 90° reflection from a Si crystal [(422) reflection with $2\theta_B = 89.682°$ for $\lambda = 0.156$ nm] placed before the detector.

It should be noted that the reflectivity with the rotated polarization is less than three to four orders of magnitude of the asymmetry ratio. The measurements of such weak signals need special precautions and thorough work with all details of the equipment. Our first experiment was not performed under optimal conditions. The most essential problem was the presence of the π-polarization ($\sim$10%) in the synchrotron radiation beam used which was reflected by our sample in the same manner as the σ-polarized part of radiation. Therefore the selected π-polarized reflectivity contained, in addition to the reflectivity with the rotated $\sigma \to \pi'$-polarization, the much larger signal of $\pi \to \pi'$-reflectivity. The subtraction of this undesired contribution led to the very poor statistics of the observed $\sigma \to \pi'$-reflectivity signal seen in Fig. 6. For details of this difficult experiment, see Andreeva *et al.* (2018a). In any case, the peak for the reflectivity with the rotated polarization at the critical angle was observed (Fig. 6). It can be attributed to the magnetic scattering on the Gd atoms because it exists only for the resonant photon energy $E_{ph} = 7930$ eV. The very small value of the 'dichroic' effect was explained not only by the small concentration of Gd atoms in the film but also by the rather thick Ti top layer, preventing penetration of the incident radiation to the Gd$_{0.23}$Co$_{0.77}$ layer. So the standing wave created in the angular region in the vicinity of the critical angle could excite only the Gd atoms in the Ti/Gd$_{0.23}$Co$_{0.77}$ interface.

Mössbauer scattering on the ^{57}Fe-containing samples is also characterized by the dichroic effect for some hyperfine components of the spectrum. In order to obtain the angular dependencies of the nuclear resonant reflectivity, the integral over reflectivity resonant spectra is measured as a function of the grazing incidence angle of the beam (Andreeva *et al.* (2018b). The measurements were made at ID18, ESRF
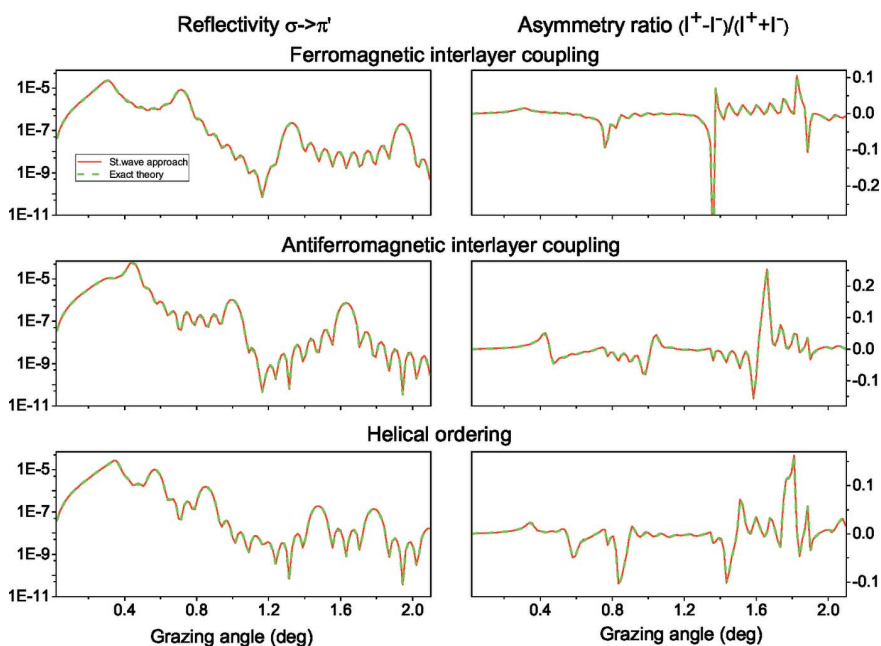
Figure 5
Angular dependencies of the rotated reflectivity (left part) and asymmetry ratio (right part), calculated by the exact theory (thin solid red lines) and by (52), (51) and (53) (thick dashed green lines) for different cases of the magnetic ordering between Gd layers: for ferromagnetic interlayer coupling [Gd(4 nm)/Ti(3 nm)]$_8$, for antiferromagnetic interlayer coupling [Gd↑(4 nm)/Ti(3 nm)/Gd↓(4 nm)/Ti(3 nm)]$_4$ and for helical ordering with magnetic period 28 nm.
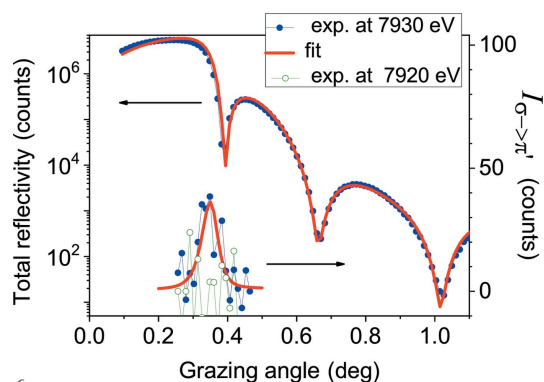

Figure 6
Experimental total reflectivity (left-hand log scale) and reflectivity with the rotated polarization (right-hand normal scale) from a Ti(10 nm)/Gd$_{0.23}$Co$_{0.77}$(250 nm)/Ti(10 nm) multilayer for E_{ph} = 7930 eV (filled blue symbols) and E_{ph} = 7920 eV (open green symbols).
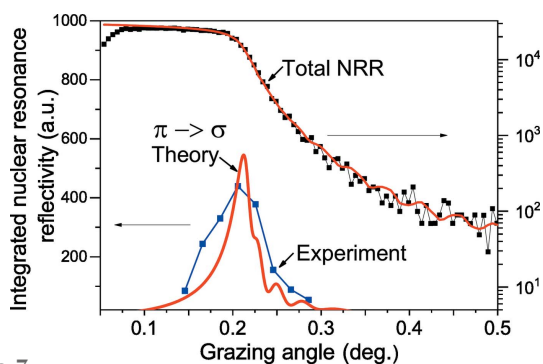

Figure 7
Nuclear resonant reflectivity (NRR) measured without polarization selection (logarithmic right-hand scale) and with the selection of the σ'-polarized reflectivity (normal left-hand scale).

(Rüffer & Chumakov, 1996), using the Synchrotron Mössbauer Source (Potapkin *et al.*, 2012*a,b*) for the sample [^{57}Fe(0.8 nm)/Cr(1.05 nm)]$_{30}$ at 4 K and the external field of 5 T in order to align the magnetizations in the ^{57}Fe layers ferromagnetically along the beam. The radiation from the Synchrotron Mössbauer Source is purely π-polarized, and the rotated polarization should have the σ-polarization state. Polarization analysis of the reflected σ-polarized radiation was carried out using an Si channel-cut crystal [two (840) reflections with $2\theta_B$ = 90.2° for λ = 0.086 nm].

The result of this first experiment (Andreeva *et al.*, 2019) is shown in Fig. 7. The essential difficulty of this experiment was the unexpected large angular divergence ($\sim$200 arcsec) of the reflected beam, caused apparently by imperfections of the surface and boundaries in the multilayer (Ragulskaya *et al.*, 2019). The Si channel-cut analyzer has an angular acceptance of only $\sim$2 arcsec; therefore, for the measurements of the reflectivity with the rotated polarization, a scan by analyzer of the reflected beam and its integration at each grazing angle was needed. However, we observed the peak at the critical angle, confirming the standing wave influence on the weak magnetic scattering with rotated polarization. With such complicated measurements, a detailed analysis of the peak shape was not possible. This will be done with improved instrumentation in the future.

7. Summary

A generalized kinematical approximation describing X-ray resonant magnetic reflectivity (XRMR) has been developed which is valid at all angles including the total reflection region. The approach takes into account the typically small value of the X-ray magnetic scattering amplitude and is based on the exact calculations of the radiation field amplitude inside the reflecting multilayer. The calculation performed with the Parratt recursive method and by propagation matrices gives identical expressions for the small magnetic contribution. We found that the squared standing waves (fourth power of the radiation field amplitude) determine the magnetic scattering at each depth.

From the described formalism the appearance of a peak near the critical angle of total reflection is predicted for the selected part of the reflectivity with rotated polarization. The first experimental test confirms this prediction. The model calculations show a full agreement of the results obtained by the described approach with the exact calculations.

There are several points stipulating the significance of the developed approach. Firstly, it can essentially speed up the calculations of the X-ray resonant magnetic reflectivity.

Secondly, the connection of the small magnetic part in the reflectivity with the squared standing waves inside the medium reveals the enhanced depth selectivity of the polarization analysis in the resonant reflectivity measurements.

Note finally that nowadays the polarization effects in X-ray reflectivity (*e.g.* Kerr rotation) become increasingly important [see, for example, Yamamoto *et al.* (2015) and Yamamoto & Matsuda (2017) developing subpicosecond time domain measurements on the platform of X-ray free-electron laser facilities]; therefore proper and simplified theoretical treatment of such effects are in high demand.

APPENDIX A
Matrix method for reflectivity calculation from an ultrathin layer

Reflectivity from an ultrathin layer in the case of scalar susceptibility $\chi(z)$ can be easily obtained using the propagation matrix method (Azzam & Bashara, 1977; Borzdov *et al.*, 1976). In the case of planar structures we use for π- or σ-polarization of radiation the scalar tangential amplitudes of the electric $E_t = |\mathbf{q} \times \mathbf{E}|$ and magnetic $H_t = -|\mathbf{q} \times \mathbf{q} \times \mathbf{H}|$ field of the plane electromagnetic wave $\exp(ikr - i\omega t)$ ($\mathbf{q}$ is the unit vector normal to the surface) to describe the variations of the radiation field amplitudes along depth z, so the Maxwell equations are reduced to the matrix differential equation (Azzam & Bashara, 1977; Born & Wolf, 1968)

$$\frac{d}{dz}\begin{pmatrix} E_t(z) \\ H_t(z) \end{pmatrix} = ik\hat{M}(z)\begin{pmatrix} E_t(z) \\ H_t(z) \end{pmatrix}, \quad (54)$$

where $k = \omega/c = 2\pi/\lambda$ is the wavevector of the monochromatic electromagnetic wave in outer space and $\hat{M}$ is the differential propagation matrix. In the case of the σ-polarization, $E_t = |\mathbf{E}| = E$ and the magnetic field of radiation $H_t = \pm\eta E$ (the $\pm$ sign refers to the waves in the direct and opposite directions), and which for, for example, σ-polarization of radiation takes the form

$$\hat{M}^{\sigma}(z) = \begin{pmatrix} 0 & 1 \\ \sin^2\theta + \chi(z) & 0 \end{pmatrix}, \quad (55)$$

where θ is the grazing angle of incidence of the plane wave and $\chi(z)$ is the susceptibility of the layered sample. The integral propagation matrix in a layer of thickness d and scalar susceptibility $\chi(z) = $ const can be easily calculated,

$$\hat{L}(d) = \begin{pmatrix} l_{11} & l_{12} \\ l_{21} & l_{22} \end{pmatrix} = \exp(ikd\,\hat{M}) = \begin{pmatrix} \cos\varphi & (i/\eta)\sin\varphi \\ i\eta\sin\varphi & \cos\varphi \end{pmatrix}, \quad (56)$$

$\eta = (\sin^2\theta + \chi)^{1/2}$, $\varphi = k\eta d$. It connects the radiation field amplitudes on the top and bottom boundaries of the layer

$$\begin{pmatrix} E_T \\ \eta_T E_T \end{pmatrix} = \hat{L}(d)\begin{pmatrix} E_0 + E_R \\ \eta_0(E_0 - E_R) \end{pmatrix}, \quad (57)$$

where the subscripts 0, R and T designate the incident, reflected and transmitted waves, $\eta_0 = (\sin^2\theta + \chi_0)^{1/2}$ and $\eta_T = (\sin^2\theta + \chi_T)^{1/2}$ are the normal components of the wavevectors

in units of ω/c in the outer medium and in the substrate. If on the outside of the layer $\chi_0 = 0$ and $\chi_T = 0$, then $\eta_0 = \eta_T = \sin\theta$. The system of two equations (57) gives the reflection amplitude

$$r = E_R/E_0 = \frac{(\eta_0 l_{22} + l_{21}) - \eta_T(\eta_0 l_{12} + l_{11})}{(\eta_0 l_{22} - l_{21}) - \eta_T(\eta_0 l_{12} - l_{11})}. \quad (58)$$

Supposing the thickness of the layer is very small, then the matrix exponential in (56) can be approximated by the expression

$$\exp(ikd\hat{M}) \cong 1 + ikd\hat{M} = \begin{pmatrix} 1 & ikd \\ ikd\eta^2 & 1 \end{pmatrix}. \quad (59)$$

If the layer is placed in a vacuum ($\chi_0 = \chi_T = 0$), substituting the elements of the integral propagation matrix from (59) into (58), the reflection amplitude from ultrathin layer takes a well known form,

$$r^d \cong \frac{\sin\theta + ikd\eta^2 - \sin^2\theta\, ikd - \sin\theta}{\sin\theta - ikd\eta^2 - \sin^2\theta\, ikd + \sin\theta} \cong \frac{ikd\chi}{2\sin\theta}. \quad (60)$$

If an ultrathin layer is placed above a reflecting mirror the boundary task (57) is modified,

$$\begin{pmatrix} E_T(1 + R) \\ \eta_0 E_T(1 - R) \end{pmatrix} = \begin{pmatrix} 1 & ikd \\ ikd\eta^2 & 1 \end{pmatrix}\begin{pmatrix} E_0 + E_R \\ \eta_0(E_0 - E_R) \end{pmatrix}, \quad (61)$$

because at the bottom boundary of the layer not only the transmitted wave is present but also the reflected wave from the substrate, $R = R^{\mathrm{substr}}\exp(iQH)$, H is the distance from substrate $Q = (4\pi/\lambda)\sin\theta$. Excluding E_T in the system of equations (61) we easily obtain R^{tot},

$$R^{\mathrm{tot}} = E_R/E_0$$

$$= \frac{-2\eta_0 R + ikd[(\eta_0^2 - \eta^2) - R(\eta_0^2 + \eta^2)]}{-2\eta_0 + ikd[(\eta^2 + \eta_0^2) + R(\eta^2 - \eta_0^2)]}$$

$$= \frac{2\eta_0 R + ikd[(\eta^2 - \eta_0^2) + R(\eta_0^2 + \eta^2)]}{2\eta_0}$$

$$\times \left\{1 + ikd\frac{[(\eta^2 + \eta_0^2) + R(\eta^2 - \eta_0^2)]}{2\eta_0}\right\}$$

$$= R + ikd\{[(\eta^2 - \eta_0^2) + 2R(\eta_0^2 + \eta^2 - \eta_0^2 + \eta_0^2)$$
$$+ R^2(\eta^2 - \eta_0^2)]/2\eta_0\}$$

$$= R(1 + 2ikd\eta_0) + ikd\frac{(\eta^2 - \eta_0^2)}{2\eta_0}(1 + 2R + R^2)$$

$$= R\exp(iQd) + r^d(1 + R)^2, \quad (62)$$

because $r^d = (\eta^2 - \eta_0^2)/2\eta_0 = ikd\chi/2\sin\theta$. Therefore the reflection from ultrathin layer $r^{d\prime}$ modified by the squared standing wave amplitude is the same as (11),

$$r^{d\prime} = [1 + R^{\mathrm{substr}}\exp(iQH)]^2\, r^d. \quad (63)$$

For consideration of some top layer above the ultrathin one we again insert the simplified designation

$$R^{\mathrm{tot}} = R_0 + \Delta_0, \quad (64)$$

and write the boundary task for this top layer (this first top layer we suppose to be vacuum, *i.e.* $\eta_0 = \sin\theta$)

$$\begin{pmatrix} E_0^d(1 + R_0 + \Delta_0) \\ \eta_0 E_0^d(1 - R_0 - \Delta_0) \end{pmatrix} = \\ \begin{pmatrix} \cos\varphi & (i/\eta_0)\sin\varphi \\ i\,\eta_0\,\sin\varphi & \cos\varphi \end{pmatrix} \begin{pmatrix} E_0^i + E_R^i \\ \eta^{\text{out}}(E_0^i - E_R^i) \end{pmatrix}. \quad (65)$$

Excluding again E_0^d in the system of equations (65) we obtain

$$\frac{(\eta_0\cos\varphi + i\eta^{\text{out}}\sin\varphi)E_0^i + (\eta_0\cos\varphi - i\eta^{\text{out}}\sin\varphi)E_R^i}{(1 + R + \Delta)} \\ - \frac{(\eta^{\text{out}}\cos\varphi + i\,\eta_0\,\sin\varphi)E_0^i - (\eta^{\text{out}}\cos\varphi - i\,\eta_0\,\sin\varphi)E_R^i}{(1 - R - \Delta)} = 0 \quad (66)$$

and

$$\{\eta_0[\exp(-i\varphi) - (R + \Delta)\exp(i\varphi)] \\ \qquad - \eta^{\text{out}}[\exp(-i\varphi) + (R + \Delta)\exp(i\varphi)]\}E_0^i \\ = \{\eta_0[-\exp(-i\varphi) + (R + \Delta)\exp(i\varphi)] \\ \qquad + \eta^{\text{out}}[-\exp(-i\varphi) - (R + \Delta)\exp(i\varphi)]\}E_R^i \quad (67)$$

and

$$E_R^i/E_0^i \\ = \frac{(\eta^{\text{out}} - \eta_0) + R\exp(2i\varphi)(\eta^{\text{out}} + \eta_0) + \Delta\exp(2i\varphi)(\eta^{\text{out}} + \eta_0)}{(\eta^{\text{out}} + \eta_0) + R\exp(2i\varphi)(\eta^{\text{out}} - \eta_0) + \Delta\exp(2i\varphi)(\eta^{\text{out}} - \eta_0)} \\ = \frac{(\eta^{\text{out}} - \eta_0) + R\exp(2i\varphi)(\eta^{\text{out}} + \eta_0) + \Delta\exp(2i\varphi)(\eta^{\text{out}} + \eta_0)}{[(\eta^{\text{out}} + \eta_0) + R\exp(2i\varphi)(\eta^{\text{out}} - \eta_0)]} \\ \times \left[1 - \frac{\Delta\exp(2i\varphi)(\eta^{\text{out}} - \eta_0)}{(\eta^{\text{out}} + \eta_0) + R\exp(2i\varphi)(\eta^{\text{out}} - \eta_0)}\right] \\ \cong \frac{(\eta^{\text{out}} - \eta_0) + R\exp(2i\varphi)(\eta^{\text{out}} + \eta_0)}{[(\eta^{\text{out}} + \eta_0) + R\exp(2i\varphi)(\eta^{\text{out}} - \eta_0)]} \quad (68) \\ + \Delta\exp(2i\varphi)\frac{(\eta^{\text{out}} + \eta_0)}{[(\eta^{\text{out}} + \eta_0) + R\exp(2i\varphi)(\eta^{\text{out}} - \eta_0)]} \\ - \Delta\exp(2i\varphi)\frac{(\eta^{\text{out}} - \eta_0)[(\eta^{\text{out}} - \eta_0) + R\exp(2i\varphi)(\eta^{\text{out}} + \eta_0)]}{[(\eta^{\text{out}} + \eta_0) + R\exp(2i\varphi)(\eta^{\text{out}} - \eta_0)]^2}.$$

The numerator at the $\Delta\exp(2i\varphi)$ term is transformed to

$$(\eta^{\text{out}} + \eta_0)[(\eta^{\text{out}} + \eta_0) + R\exp(2i\varphi)(\eta^{\text{out}} - \eta_0)] \\ - (\eta^{\text{out}} - \eta_0)[(\eta^{\text{out}} - \eta_0) + R\exp(2i\varphi)(\eta^{\text{out}} + \eta_0)] = 4\eta_0\eta^{\text{out}}$$

and

$$\frac{(\eta^{\text{out}} - \eta_0)}{(\eta^{\text{out}} + \eta_0)} = r_f, \qquad \frac{4\eta_0\eta^{\text{out}}}{(\eta^{\text{out}} + \eta_0)^2} = t_f t_f', \quad (69)$$

where r_f, t_f, t_f' are the Fresnel amplitudes of the reflection and transmission at the boundary between vacuum and outer medium. Finally, we obtain, similar to (14) and (15),

$$R^{\text{out}} = \frac{E_R^i}{E_0^i} = \frac{r_f + R\exp(2i\varphi)}{1 + r_f R\exp(2i\varphi)} + \left\{\exp(2i\varphi)\frac{t_f t_f'}{[1 + r_f R\exp(2i\varphi)]^2}\right. \\ \left. \times [1 + R^{\text{substr}}\exp(iQH)]^2 r^d\right\}. \quad (70)$$

The propagation matrices allow the necessity to calculate the radiation field successively at each intermediate boundary to be avoided, but to calculate the radiation field at the position of the ultrathin layer using the integral propagation matrix for the whole stack above the ultrathin layer. We use such a matrix in the general form

$$\hat{L} = \begin{pmatrix} l_1 & l_2 \\ l_3 & l_4 \end{pmatrix}, \quad (71)$$

and write down the boundary task as follows,

$$\begin{pmatrix} E_0^d(1 + R + \Delta) \\ \eta_0 E_0^d(1 - R - \Delta) \end{pmatrix} = \begin{pmatrix} l_1 & l_2 \\ l_3 & l_4 \end{pmatrix}\begin{pmatrix} E_0^{\text{out}} + E_R^{\text{out}} \\ \eta^{\text{out}}(E_0^{\text{out}} - E_R^{\text{out}}) \end{pmatrix}. \quad (72)$$

Calculation of the total reflectivity R^{out} is performing similar to (68),

$$R^{\text{out}} = \frac{E_R^{\text{out}}}{E_0^{\text{out}}} \\ = \frac{\eta_0(1 - R - \Delta)(l_1 + \eta^{\text{out}}l_2) - (1 + R + \Delta)(l_3 + \eta^{\text{out}}l_4)}{-\eta_0(1 - R - \Delta)(l_1 - \eta^{\text{out}}l_2) + (1 + R + \Delta)(l_3 - \eta^{\text{out}}l_4)} \\ = \frac{\eta_0(1 - R)(l_1 + \eta^{\text{out}}l_2) - (1 + R)(l_3 + \eta^{\text{out}}l_4)}{-\eta_0(1 - R)(l_1 - \eta^{\text{out}}l_2) + (1 + R)(l_3 - \eta^{\text{out}}l_4)} \\ - \Delta\Big[\big\{[\eta_0(1 - R)(l_1 + \eta^{\text{out}}l_2) - (1 + R)(l_3 + \eta^{\text{out}}l_4)] \\ \times [(\eta_0 l_1 - \eta_0\eta^{\text{out}}l_2 + l_3 - \eta^{\text{out}}l_4)]\big\} \\ \big/[-\eta_0(1 - R)(l_1 - \eta^{\text{out}}l_2) + (1 + R)(l_3 - \eta^{\text{out}}l_4)]^2\Big] \\ - \Delta\Big[\big\{[-\eta_0(1 - R)(l_1 - \eta^{\text{out}}l_2) + (1 + R)(l_3 - \eta^{\text{out}}l_4)] \\ \times [(\eta_0 l_1 + \eta_0\eta^{\text{out}}l_2 + l_3 + \eta^{\text{out}}l_4)]\big\} \\ \big/[-\eta_0(1 - R)(l_1 - \eta^{\text{out}}l_2) + (1 + R)(l_3 - \eta^{\text{out}}l_4)]^2\Big]. \quad (73)$$

Using the designations

$$a = (l_1 + l_3/\eta_0), \qquad b = (l_1 - l_3/\eta_0), \\ c = (l_4 + \eta_0 l_2), \qquad u = (l_4 - \eta_0 l_2), \quad (74)$$

we transform (73) to the following expression,

$$R^{\text{out}} = \frac{(u\eta^{\text{out}} - b\eta_0) + R(c\eta^{\text{out}} + a\eta_0)}{(u\eta^{\text{out}} + b\eta_0) + R(c\eta^{\text{out}} - a\eta_0)} \\ + \Delta\frac{4\eta_0\eta^{\text{out}}(l_1 l_4 - l_2 l_3)}{[(u\eta^{\text{out}} + b\eta_0) + R(c\eta^{\text{out}} - a\eta_0)]^2}. \quad (75)$$

If $\hat{L}$ is presented by (56) then $u = b = \exp(-i\varphi)$, $a = c = \exp(i\varphi)$ and for one upper layer we obtain (70) and (15).

The expression (75) can essentially speed up the calculations of reflectivity from an ultrathin layer or for small resonant contributions.

and R. Rüffer (ESRF) for help with experiments, and Yu. A. Babanov (IMP UB RAS), D. Ponomarev (IMP UB RAS), G. V. Kurlyandskaya (UrFU) and A. V. Svalov (UrFU) for the provided samples.

References

Andreeva, M. A., Baulin, R. A., Borisov, M. M., Gan'shina, E. A., Kurlyandskaya, G. V., Mukhamedzhanov, E., Repchenko, Y. L. & Svalov, A. V. (2018*a*). *J. Exp. Theor. Phys.* **126**, 802–810.

Andreeva, M., Baulin, R., Chumakov, A., Kiseleva, T. & Rüffer, R. (2019). *Condens. Matter*, **4**, 8.

Andreeva, M. A., Baulin, R. A., Chumakov, A. I., Rüffer, R., Smirnov, G. V., Babanov, Y. A., Devyaterikov, D. I., Milyaev, M. A., Ponomarev, D. A., Romashev, L. N. & Ustinov, V. V. (2018*b*). *J. Synchrotron Rad.* **25**, 473–483.

Andreeva, M. A. & Lindgren, B. (2002). *JETP Lett.* **76**, 704–706.

Andreeva, M. A. & Lindgren, B. (2005). *Phys. Rev. B*, **72**, 125422.

Andreeva, M. A. & Repchenko, Yu. L. (2013). *Crystallogr. Rep.* **58**, 1037–1042.

Andreeva, M. A. & Repchenko, Yu. L. (2017). http://kftt.phys.msu.ru/index.php?id=47.

Andreeva, M. A. & Rosete, C. (1986). *Vestn. Mosk. Univ. Fiz.* **41**(3), 57.

Andreeva, M. & Smekhova, A. (2006). *Appl. Surf. Sci.* **252**, 5619–5621.

Andreeva, M., Smekhova, A., Lindgren, B., Björck, M. & Andersson, G. (2006). *J. Magn. Magn. Mater.* **300**, e371–e374.

Azzam, R. & Bashara, N. (1977). *Ellipsometry and Polarized Light.* Amsterdam: North-Holland.

Barkovskii, L. M., Borzdov, G. N. & Fedorov, F. I. (1983). *Wave Operators in Optics*, Preprint of Institute of Physics, Belarusian Academy of Science, Minsk, No. 304.

Baron, A. Q. R., Arthur, J., Ruby, S. L., Chumakov, A. I., Smirnov, G. V. & Brown, G. S. (1994). *Phys. Rev. B*, **50**, 10354–10357.

Bedzyk, M. J., Bommarito, G. M. & Schildkraut, J. S. (1989). *Phys. Rev. Lett.* **62**, 1376–1379.

Bergmann, A., Grabis, J., Nefedov, A., Westerholt, K. & Zabel, H. (2006). *J. Phys. D Appl. Phys.* **39**, 842–850.

Beutier, G., Collins, S. P., Dimitrova, O. V., Dmitrienko, V. E., Katsnelson, M. I., Kvashnin, Y. O., Lichtenstein, A. I., Mazurenko, V. V., Nisbet, A. G. A., Ovchinnikova, E. N. & Pincini, D. (2017). *Phys. Rev. Lett.* **119**, 167201.

Blume, M. & Gibbs, D. (1988). *Phys. Rev. B*, **37**, 1779–1789.

Bohr, J. (1990). *J. Magn. Magn. Mater.* **83**, 530–534.

Bohr, J., Gibbs, D., Axe, J. D., Moncton, D. E., D'amico, K. L., Majrzak, C. F., Kwo, J., Hong, M., Chien, C. L. & Jensen, J. (1989). *Physica B*, **159**, 93–105.

Born, M. & Wolf, E. (1968). *Principles of Optics.* New York: Pergamon Press.

Borzdov, G. N., Barkovskii, L. M. & Lavrukovich, V. I. (1976). *Zh. Prikl. Spektrosk.* **25**, 526.

Bourzami, A., Lenoble, O., Féry, Ch., Bobo, J. F. & Piecuch, M. (1999). *Phys. Rev. B*, **59**, 11489–11494.

Brouder, Ch. (1990). *J. Phys. Condens. Matter*, **2**, 701–738.

Brück, S., Schütz, G., Goering, E., Ji, X. & Krishnan, K. M. (2008). *Phys. Rev. Lett.* **101**, 126402.

Brückel, T., Lippert, M., Köhler, T., Schneider, J. R., Prandl, W., Rilling, V. & Schilling, M. (1996). *Acta Cryst.* A**52**, 427–437.

Caciuffo, R., Paolasini, L., Sollier, A., Ghigna, P., Pavarini, E., van den Brink, J. & Altarelli, M. (2002). *Phys. Rev. B*, **65**, 174425.

Collins, S. P. (1999). *J. Phys. Condens. Matter*, **11**, 1159–1175.

Elzo, M., Jal, E., Bunau, O., Grenier, S., Joly, Y., Ramos, A. Y., Tolentino, H. C. N., Tonnerre, J. M. & Jaouen, N. (2012). *J. Magn. Magn. Mater.* **324**, 105–112.

Elzo, M., Moubah, R., Blouzon, C., Sacchi, M., Grenier, S., Belkhou, R., Dhesi, S., Colson, D., Torres, F., Kiwi, M., Viret, M. & Jaouen, N. (2015). *Phys. Rev. B*, **91**, 014402.

Fernandez, V., Vettier, C., de Bergevin, F., Giles, C. & Neubeck, W. (1998). *Phys. Rev. B*, **57**, 7870–7876.

Freeland, J. W., Chakhalian, J., Boris, A. V., Tonnerre, J.-M., Kavich, J. J., Yordanov, P., Grenier, S., Zschack, P., Karapetrova, E., Popovich, P., Lee, H. N. & Keimer, B. (2010). *Phys. Rev. B*, **81**, 094414.

Geissler, J., Goering, E., Justen, M., Weigand, F., Schütz, G., Langer, J., Schmitz, D., Maletta, H. & Mattheis, R. (2001). *Phys. Rev. B*, **65**, 020405.

Gibbs, D., Harshman, D. R., Isaacs, E. D., McWhan, D. B., Mills, D. & Vettier, C. (1988). *Phys. Rev. Lett.* **61**, 1241–1244.

Gibert, M., Viret, M., Zubko, P., Jaouen, N., Tonnerre, J.-M., Torres-Pardo, A., Catalano, S., Gloter, A., Stéphan, O. & Triscone, J.-M. (2016). *Nat. Commun.* **7**, 11227.

Goulon, J., Rogalev, A., Wilhelm, F., Goulon-Ginet, C., Carra, P., Marri, I. & Brouder, Ch. (2003). *J. Exp. Theor. Phys.* **97**, 402–431.

Höchst, H., Rioux, D., Zhao, D. & Huber, D. L. (1997). *J. Appl. Phys.* **81**, 7584–7588.

Höchst, H., Zhao, D. & Huber, D. L. (1996). *Surf. Sci.* **352–354**, 998–1002.

Hosoito, N., Ohkochi, T., Kodama, K. & Yamagishi, R. (2009). *J. Phys. Soc. Jpn*, **78**, 094716.

Ishimatsu, N., Hashizume, H., Hamada, S., Hosoito, N., Nelson, C. S., Venkataraman, C. T., Srajer, G. & Lang, J. C. (1999). *Phys. Rev. B*, **60**, 9596–9606.

Jaouen, N., van der Laan, G., Johal, T. K., Wilhelm, F., Rogalev, A., Mylonas, S. & Ortega, L. (2004). *Phys. Rev. B*, **70**, 094417.

Kao, C. C., Chen, C. T., Johnson, E. D., Hastings, E. D., Lin, H. J., Ho, G. H., Meigs, G., Brot, J. M., Hulbert, S. L., Idzerda, Y. U. & Vettier, C. (1994). *Phys. Rev. B*, **50**, 9599–9602.

Kim, S.-K. & Kortright, J. B. (2001). *Phys. Rev. Lett.* **86**, 1347–1350.

Kortright, J. & Rice, M. (1996). *Rev. Sci. Instrum.* **67**, 3353.

Kortright, J. B. & Kim, S.-K. (2000). *Phys. Rev. B*, **62**, 216.

Kravtsov, E., Haskel, D., te Velthuis, S. G. E., Jiang, J. S. & Kirby, B. J. (2009). *Phys. Rev. B*, **79**, 1334438.

Laan, G. (2013). *J. Phys. Conf. Ser.* **430**, 012127.

Langridge, S., Lander, G. H., Bernhoeft, N., Stunault, A., Vettier, C., Grübel, G., Sutter, C., de Bergevin, F., Nuttall, W. J., Stirling, W. G., Mattenberger, K. & Vogt, O. (1997). *Phys. Rev. B*, **55**, 6392–6398.

McWhan, D. B., Vettier, C., Isaacs, E. D., Ice, G. E., Siddons, D. P., Hastings, J. B., Peters, C. & Vogt, O. (1990). *Phys. Rev. B*, **42**, 6007–6017.

Mertins, H., Abramsohn, D., Gaupp, A., Schäfers, F., Gudat, W., Zaharko, O., Grimmer, H. & Oppeneer, P. M. (2002). *Phys. Rev. B*, **66**, 184404.

Mertins, H., Oppeneer, P. M., Kunes, J., Gaupp, A., Abramsohn, D. & Schäfers, F. (2001). *Phys. Rev. Lett.* **87**, 047401.

Mertins, H., Schäfers, F., Le Cann, X., Gaupp, A. & Gudat, W. (2000). *Phys. Rev. B*, **61**, R874–R877.

Mertins, H. C., Valencia, S., Abramsohn, D., Gaupp, A., Gudat, W. & Oppeneer, P. M. (2004). *Phys. Rev. B*, **69**, 064407.

Moncton, D. E., Gibbs, D. & Bohr, J. (1986). *Nucl. Instrum. Methods Phys. Res. A*, **246**, 839–844.

Natoli, C. R., Brouder, Ch., Sainctavit, Ph., Goulon, J., Goulon-Ginet, Ch. & Rogalev, A. (1998). *Eur. Phys. J. B*, **4**, 1.

Neubeck, W., Vettier, C., Fernandez, V., de Bergevin, F. & Giles, C. (1999). *J. Appl. Phys.* **85**, 4847–4849.

Odintsova, E. E. & Andreeva, M. A. (2010). *J. Surface Invest.* **4**, 913.

Oppeneer, P. (2001). *Magneto-Opt. Kerr Spectra. Handb. Magn. Mater.* **13**, 229.

Ott, H., Schüler-Langeheine, C., Schierle, E., Kaindl, G. & Weschke, E. (2006). *Appl. Phys. Lett.* **88**, 212507.

Parratt, L. G. (1954). *Phys. Rev.* **95**, 359–369.

Pleshanov, N. K. (1994). *Z. Phys. B Condens. Matter*, **94**, 233–243.

Potapkin, V., Chumakov, A. I., Smirnov, G. V., Celse, J.-P., Rüffer, R., McCammon, C. & Dubrovinsky, L. (2012*b*). *J. Synchrotron Rad.* **19**, 559–569.

Potapkin, V., Chumakov, A. I., Smirnov, G. V., Rüffer, R., McCammon, C. & Dubrovinsky, L. (2012*a*). *Phys. Rev. A*, **86**, 053808.

Ragulskaya, A. V., Andreeva, M. A., Rogachev, M. A. & Yakunin, S. N. (2019). *Superlattices Microstruct.* **125**, 16–25.

Rüffer, R. & Chumakov, A. I. (1996). *Hyperfine Interact.* **97–98**, 589–604.

Rühm, A., Toperverg, B. P. & Dosch, H. S. (1999). *Phys. Rev. B*, **60**, 16073–16077.

Schütz, G., Knülle, V. & Ebert, H. (1994). In *Resonant Anomalous X-ray Scattering*, edited by G. Materlik, C. J. Sparks & K. Fischer. Elsevier Science.

Sessoli, R., Boulon, M.-E., Caneschi, A., Mannini, M., Poggini, L., Wilhelm, F. & Rogalev, A. (2014). *Nat. Phys.* **11**, 69–74.

Sève, L., Jaouen, N., Tonnerre, J. M., Raoux, D., Bartolomé, F., Arend, M., Felsch, W., Rogalev, A., Goulon, J., Gautier, C. & Bérar, J. F. (1999). *Phys. Rev. B*, **60**, 9662–9674.

Siddons, D. P., Hart, M., Amemiya, Y. & Hastings, J. B. (1990). *Phys. Rev. Lett.* **64**, 1967–1970.

Sorg, C., Scherz, A., Baberschke, K., Wende, H., Wilhelm, F., Rogalev, A., Chadov, S., Minár, J. & Ebert, H. (2007). *Phys. Rev. B*, **75**, 064428.

Stepanov, S. A. & Sinha, S. K. (2000). *Phys. Rev. B*, **61**, 15302–15311.

Stöhr, J. (1995). *J. Electron Spectrosc. Relat. Phenom.* **75**, 253–272.

Svalov, A. V., Kurlyandskaya, G. V., Balymov, K. G. & Vas'kovskii, V. O. (2016). *Phys. Metals Metallogr.* **117**, 876.

Takahashi, M., Usuda, M. & Igarashi, J. (2003). *Phys. Rev. B*, **67**, 064425.

Toellner, T. L., Sturhahn, W., Röhlsberger, R., Alp, E. E., Sowers, E. E. & Fullerton, E. E. (1995). *Phys. Rev. Lett.* **74**, 3475–3478.

Tonnerre, J. M., Sève, L., Raoux, D., Soullié, G., Rodmacq, B. & Wolfers, P. (1995). *Phys. Rev. Lett.* **75**, 740–743.

Valvidares, S. M., Quirós, C., Mirone, A., Tonnerre, J.-M., Stanescu, S., Bencok, P., Souche, Y., Zárate, L., Martín, I., Vélez, M., Brookes, N. B. & Alameda, J. M. (2008). *Phys. Rev. B*, **78**, 064406.

Yamamoto, Sh. & Matsuda, I. (2017). *Appl. Sci.* **7**, 662.

Yamamoto, Sh., Taguchi, M., Someya, T., Kubota, Y., Ito, S., Wadati, H., Fujisawa, M., Capotondi, F., Pedersoli, E., Manfredda, M., Raimondi, L., Kiskinova, M., Fujii, J., Moras, P., Tsuyama, T., Nakamura, T., Kato, T., Higashide, T., Iwata, S., Yamamoto, S., Shin, S. & Matsuda, I. (2015). *Rev. Sci. Instrum.* **86**, 083901.

Zak, J., Moog, E. R., Liu, C. & Bader, S. D. (1991). *Phys. Rev. B*, **43**, 6423–6429.